CORONAL STRUCTURES OBSERVED AT METRIC WAVELENGTHS WITH THE NANÇAY RADIOHELIOGRAPH

C. E. ALISSANDRAKIS* and P. LANTOS

LA 324, Meudon Observatory

and

E. NICOLAIDIS

Section of Astrophysics, Astronomy and Mechanics, Department of Physics, University of Athens

(Received 13 November, 1984; in revised form 4 March, 1985)

Abstract. We present and discuss two-dimensional maps of the Sun at 169 MHz, obtained with the Nançay radioheliograph used as an Earth rotation aperture synthesis instrument. The maps have been computed on the basis of about 6 hr of one-dimensional observations by the east–west and the north–south arrays of the radioheliograph and have a resolution of 1.5′ by 4.2′ for a solar declination near 23°. In addition to a broad background component, the maps show several features both brighter and darker than the background. Some of the bright features are sources of noise storm continua, as evidenced by their positions relative to active regions and by the occurrence of type I bursts. Weaker emission regions are apparently associated with neutral lines of the photospheric magnetic field. We found no sources associated with extended quiescent filaments. Some of the depressions on the maps correspond to coronal holes both in the equatorial region and near the poles, while the more shallow ones may be arch regions with low electron temperature and/or emission measure. The distribution of brightness temperature at a height of 0.15 solar radii above the photospheric limb shows a gross similarity with coronal green line observations. The present results indicate that the notion of the slowly varying component at metric wavelengths may have to be reexamined, since sources of different nature may have been grouped in this component in the past.

1. Introduction

Solar radio emission is traditionally divided into three components: quiet Sun emission, the slowly varying component and burst emission (Kundu, 1965). The slowly varying component (SVC) corresponds to fairly stable sources, rotating with the Sun. The quiet Sun, which is generally obtained as the lower envelope of one-dimensional or two-dimensional maps, is the solar background emission, while the burst emission is the short time-scale component of the emission.

In agreement with the X-ray and EUV observations, the metric quiet Sun emission is divided into coronal holes and coronal arches (Dulk and Sheridan, 1974; Lantos and Avignon, 1975; Chiuderi-Drago *et al.*, 1977; Trottet and Lantos, 1978). The brightness temperature of the coronal holes is low; various observers using different methods are in good agreement and give values of $6.4 \pm 0.8 \times 10^5$ K near 169 MHz (see compilation by Lantos, 1980), while a long-term analysis by the lower envelope method (Lantos and Avignon, 1975) indicated that there is no variation of the brightness temperature of coronal holes during the solar cycle. On the other hand, the measurements of brightness

* On leave from the section of Astrophysics, Astronomy and Mechanics, Department of Physics, University of Athens.

Solar Physics **97** (1985) 267–282. 0038–0938/85.15

temperature in arch regions, compiled by Lantos (1980), show significant variations between 7×10^5 K and 1.2×10^6 K.

The origin of the metric SVC is more controversial. Moutot and Boischot (1961) as well as Leblanc (1970), using observations obtained with the Nançay east–west interferometer have associated the enhancement of the quiet Sun emission with active region plages and have interpreted it in terms of thermal emission. On the contrary Axisa *et al.* (1971), also on the basis of one-dimensional Nançay observations during the minimum of the solar cycle, have associated the SVC sources with Hα filaments seen on synoptic maps and have interpreted them in terms of thermal emission originating in coronal streamers. Dulk and Sheridan (1974), using two-dimensional maps from Culgoora, have associated one bright region with 'quiescent filament and not with plage or bright region on microwave or UV maps'.

In this paper we present preliminary results on the solar emission at 169 MHz, based on two-dimensional maps obtained with the Nançay radioheliograph, which has been used for the first time as an Earth rotation aperture synthesis instrument. The requirements of the synthesis method limit our ability to map sources with significant variations during the six hours of observations. The puzzling origin of the slowly varying component at metric wavelengths is discussed within the framework of analysis of the metric emission, which shows how questionnable the widely accepted classification into quiet Sun, slowly varying component and burst emission may be.

2. Observations and Data Reduction

The observations were obtained with the Nançay radioheliograph at 169 MHz (Radioheliograph group, 1977, 1983). The instrument consists of two independent arrays, one in the east–west direction and one in the north–south direction. Each array operates as a fan beam synthesis instrument, normally at a rate of 25 images per second in total intensity and circular polarization.

The east–west array consists of 16 antennas of 3 m diameter and 2 antennas of 10 m diameter. Each large antenna is correlated with each small, resulting in 32 two-element interferometers with baselines from 100 m to 3200 m (56 to 1800 wavelengths) in steps of 100 m. The north–south array consists of 11 antennas of 5 m diameter; each antenna is correlated with the central antenna of the E–W array forming 11 two-element interferometers with baselines from 109 m to 1195 m (61–670 wavelengths). The antennas are stearable within $\pm$ 3 hr from the central meridian, which limits the duration of the observation to a maximum of 6 hr.

The amplitude and phase calibration is done by observing celestial sources of known intensity distribution such as Cygnus A, since strong point sources are rare at 169 MHz. Until recently the amplitude calibration was performed independently for the E–W and N–S arrays and there was no absolute calibration; the absolute calibration is done by measuring the total flux of the Sun with the Nançay interferometer, which is accurate to about 10%.

The E–W and N–S scans of the radioheliograph are sufficient for the measurement

of position and size as well as for the study of the time evolution of small sources such as bursts; however, they are not suitable for the study of large sources, such as the sources of the slowly varying component or the quiet Sun background. Therefore we developed a method for constructing two-dimensional maps from the one-dimensional observations of the two arrays. The method, which has been described in detail by Alissandrakis (1983), is essentially the Earth rotation aperture synthesis (see for example Fomalont and Wright, 1974) with some modifications due to the characteristics of the solar emission at meter wavelengths as well as of the instrument. In the rest of this section we will present the method and discuss its advantages and its limitations.

Earth rotation aperture synthesis has already been used successfully for the computation of active regions maps at cm wavelengths (e.g. Kundu and Alissandrakis, 1975). In such observations the visibility function is recorded on magnetic tape, subsequently it is calibrated and finally the map is obtained as the Fourier transform (FT) of the visibility. In our case we start with the E–W and N–S scans obtained during a 6 hr observing period, which are Fourier transformed to recover the original visibility. This procedure has been adopted in order not to interfere with the normal operation of the instrument; moreover all the information obtainable by the instrument is contained in the one-dimensional scans.

The quality of a synthesis map depends on the completeness of sampling of the visibility function on the $u - v$ plane. Incomplete sampling in the radial direction results in grating rings and limits the ability of the system to detect extended sources. Incomplete sampling in the angular direction results in a non-elliptical beam shape with strong negative sidelobes. Finally, the coverage of the $u - v$ plane up to a maximum distance from the origin limits the resolution of the map.

As the Earth rotates, a two-element interferometer samples the visibility function along an ellipse. For an E–W interferometer observing for ± 6 hr around the central meridian passage of the source this results in a complete angular coverage of the $u - v$ plane. Since the radioheliograph operates only for ± 3 hr around the central meridian passage, the angular coverage of the $u - v$ plane by the E–W array alone is incomplete. Part of the missing angles are sampled by the N–S array, however there is still a part of the $u - v$ plane which is not sampled. The coverage of the $u - v$ plane is shown in Figure 1 for a source with a declination of 20°. The angular gap is largest (52°) at zero declination, when the E–W array provides no angular coverage; at the maximum solar declination the gap is still 36° wide and it drops to zero for a source at the pole of the celestial sphere.

The resolution of the E–W array (full width at half power of the fan beam) is 1.15′ while that of the N–S array is $2.9/\cos(\phi - \delta)$, where $\phi = 47° 22' 48''$ is the latitude of the instrument and δ the declination of the source. In the case of the two-dimensional maps the resolution is slightly less than that; for example the resolution is 1.5′ E–W by 4.2′ N–S for a declination of 23°.

Due to the incomplete coverage of the $U - V$ plane in the radial direction the beam pattern shows grating rings; in the E–W direction the radius of first grating ring is 61.1′, while in the N–S direction it is $56.8'/\cos(\phi - \delta)$. The grating response limits the ability

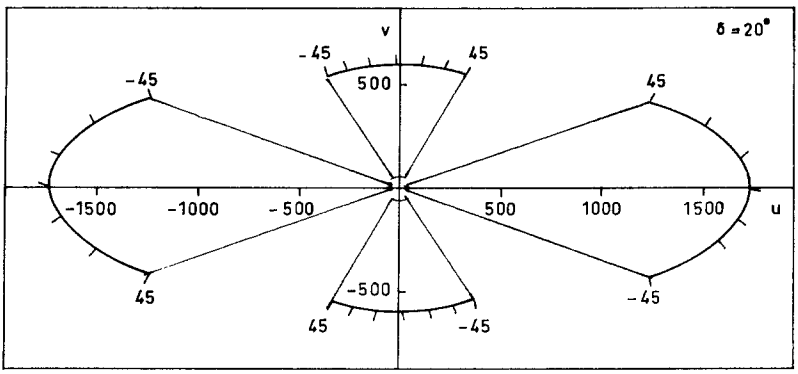

Fig. 1. Sampling of the $u - v$ plane by the shortest and the longest baseline of the east–west and the north–south branch of the Nançay radioheliograph for a source at a declination of 20°. The range of hour angle is from $-45°$ to 45° and the tickmarks on the curves are every 15°. The units on the axes are in wavelengths.

of the instrument to detect extended sources, such as those having non-zero brightness at distances from the center of the field comparable to the radius of the first grating ring. Notice that the radius of the grating ring is about twice the photospheric diameter so that disk, as well as limb structures which are located at low heights above the photosphere will not suffer from this problem. However the background coronal emission may have a considerable extent, consequently the measurements of its intensity at large distances from the photospheric limb must be done with extreme care.

The computation of the maps is done in four steps. The application of synthesis requires that the source should be fairly constant in the cource of the 6 hr long observation, consequently we can only use scans free of burst activity. Due to the large number of bursts (particularly of type I) at metric wavelengths, a preliminary selection of days with low activity is necessary. A further requirement is that the declination of the Sun should be fairly high (larger than about 15°) in order to obtain maps with acceptable resolution in the N–S direction and good angular coverage in the $U - V$ plane. After the preliminary selection of observations a computer program deletes automatically scans which contain bursts, on the basis of the maximum intensity and the total flux of each scan. The selected scans are integrated over a 3 min interval. The integration time is short enough to avoid distortion of the map due to the rotation of the baseline; values of up to 13 min can be used without undesirable effects (Alissandrakis, 1983). The same program computes the relative calibration factor between the E–W and N–S arrays by comparing the total flux of the corresponding scans. Further, the integrated scans are Fourier transformed and the original visibility is recovered.

Besides the time variations, an additional cause of distortion of the maps is the motion of a source with respect to the fringe stopping center. Although the radioheliograph tracks the Sun, there is a residual motion due to solar rotation; for a source at the center of the disk at a height of 0.3 solar radii, this amounts to 1.2 arc min over the six hours of observation, which is slightly less than the E–W resolution of the maps. Due to the non-uniform effect of the rotation over the solar disk, no correction is done.

The dominant component of the two-dimensional solar map is the broad quiet Sun background. This has the following undesirable effects if a map is computed by a straight forward FT of the visibility: the grating lobes of the background component are so wide that they partly merge with the solar image; moreover it is impossible to use conventional 'cleaning' methods because the solar image is much larger than the beam pattern. It is therefore necessary to remove this component before the computation of the map, which requires the fit of a model source to the visibility function; the fit is done in the second step of the data processing. The model source which we found more suitable for this purpose is the convolution of a flat elliptical disk with a gaussian; on the $u - v$ plane its FT is the product of a Bessel function with a gaussian, so that the parameters of the broad source can be determined by conventional least square fit methods. Due to the large size of the source only the shortest two baselines are used for the fit. We should note that although the subtraction of the broad source improves the quality of the maps, the source itself does not have a direct physical meaning; it does not necessarily represent the 'quiet Sun' component, which is usually obtained with the lower envelope method.

In the third step of data processing the visibility function, after the subtraction of the broad background source, is placed in a rectangular grid and subsequently its Fourier transform is computed, using a fast FT routine; this gives the 'dirty' map of the Sun. Simultaneously with the dirty map the program computes the 'dirty beam pattern' which is the response of the array (under the assumption of perfect amplitude and phase calibration) to a point source.

The last step of the processing is an attempt to free the dirty map of the sidelobes and the grating rings; effectively this corresponds to filling the gaps in the $u - v$ plane. This operation is not easy because the problem does not have a unique solution. The subtraction of the broad background source before the computation of the map is already a step in this direction. The widely used method of 'cleaning', i.e. the decomposition of the dirty map into point sources (Högbom, 1974) is used subsequently. Approximately, 300 point sources are subtracted from the dirty map before a residual level of 10% is reached. This number should be compared to the number of independent data points provided by the observations; since 32 complex data points are observed by the E–W array and 11 by the N–S array, we have roughly 1300 independent points on the map. Consequently, the number of 300 point sources is within the observational limits. After cleaning the dirty map the model background source is added back to give the final map.

The quality of the maps depends upon a number of factors, the more important of which are the accuracy of the amplitude and phase calibration, the duration of the observation and the stability of the sources during the observation. Improper calibration will distort the dirty beam pattern and will produce spurious sources. Observations of long duration permit a more complete sampling of the $u - v$ plane and result in a beam pattern with weaker negative sidelobes. Finally sources with variable intensity will be distorted (Kundu *et al.*, 1977) and may even produce negative sidelobes. The last problem is important in the presence of noise storm sources of strong to moderate

intensity which are frequently variable; sidelobes from such sources may be stronger than the sources of quiet Sun emission and they can ruin an observation unless the sources are located far from the center of the disk. The quality of a given map can be judged from the level of regions of negative intensity as well as from the rugged appearence of the low intensity contours; on the basis of that information we estimate that the level of confidence for brightness temperature variations is about, 5×10^4 K, which corresponds to a dynamic range better than a factor of 20.

3. Results and Discussion

In this section we will present and discuss the maps obtained during two relatively quiet periods, between June 29 and July 3, 1980 and from July 28 to August 5, 1980. A comparison of our maps of the first period with those of Culgoora at 160 MHz (courtesy of R. Stewart) showed a good correspondence of the bright and dark regions; this gives additional confidence to our method, since the Culgoora maps are produced by a more conventional method. Figure 2 shows the 169 MHz maps from July 28 to August 2; the map of July 29 has been computed with only 1.5 hr of observations and it is consequently of inferior quality.

In agreement with Dulk and Sheridan (1974) our maps show an intensity distribution with a flat top, a rapid drop near the half maximum level and an extended low brightness emission.

The brightness temperature of the flat top is 9×10^5 K, while the accuracy of our absolute calibration is about 10%. The lowest contour of the maps, at 10^5 K, extends up to 1.8 solar radii in the east–west direction and up to 1.5 solar radii in the north–south. The ratio of the axes is about 1.25 at all levels with significant variation from day to day; we should note, however that this ratio may be affected by errors in the determination of the relative calibration factor between the E–W and the N–S arrays of the radioheliograph.

The maps in Figure 2 show both regions of emission as well as depressions with respect to the background. The depressions are few and quite shallow. On the other hand there are numerous emission sources; some are fairly bright, such as region *A* from July 28 to 31 and region *B* near the limb on August 1 and 2, but most are just 5×10^4 to 2×10^5 K brighter than the surrounding background. A comparison of the 169 MHz maps with Hα spectroheliograms showed no obvious correspondence between the emission sources and Hα features. Contrary to the observation of Dulk and Sheridan (1974), extended quiescent filaments, such as those drawn on the map of July 28, show no associated metric emission; we should note that the large filament on the north hemisphere disappeared between July 29 and 30, without any detectable change on the 169 MHz maps. Similarly, no radioemission associated with prominent filaments was observed in the period June 29–July 3, 1980. A close examination of the Culgoora maps of Dulk and Sheridan (1974) shows that although at 80 MHz there was indeed a source above an Hα filament, the association is less apparent at 160 MHz. On the other hand, Axisa *et al.* (1971) have published that the thermal sources were linked to the presence

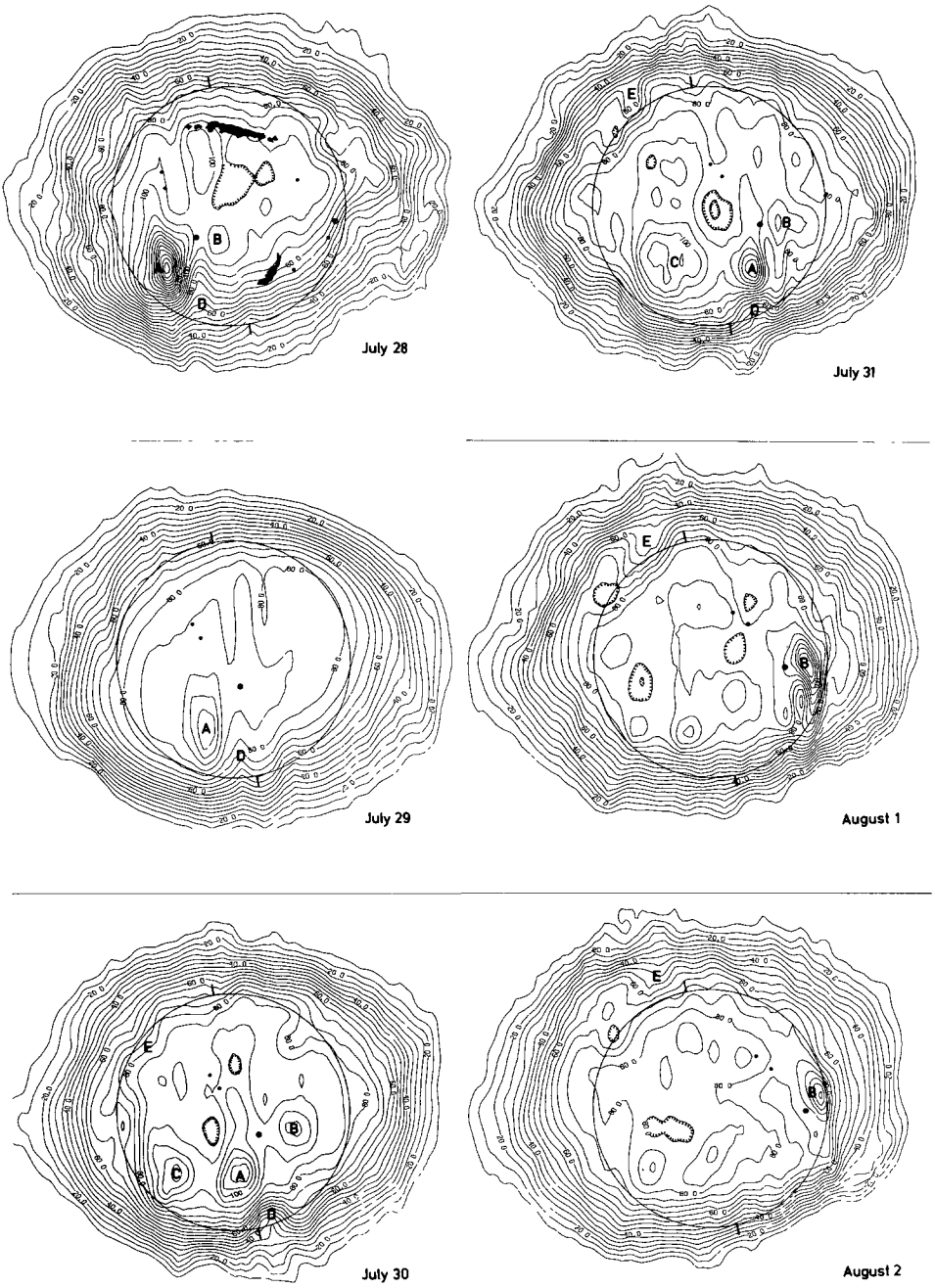

Fig. 2. Two-dimensional synthesis maps at 169 MHz obtained with the Nançay radioheliograph from July 28 to August 3, 1980. The contour labels are in units of 10^4 K. Hatched contours show regions of lower than the background brightness temperature. The circle corresponds to the photospheric limb The maps are oriented with the celestial north up, while the position of the solar north and south poles is shown by small marks. Small and large filled circles show the position of small and large sunspots. On the July 28 map we have drawn two large quiescent filaments.

of filaments and not the inverse. In any case further two-dimensional observations are needed in order to reach a more complete view on the filament counterpart at metric wavelengths.

The position of sunspots is indicated on the maps of Figure 2 by black dots, small or large, depending on the size of the spot. We do not find metric emission above active regions with sunspots; this is also true for the case of brightest Hα plages without sunspots. Thus we do not observe thermal emission from 'coronal condensations' above active regions. The brightest features appear to be related with the active regions, however they are clearly displaced with respect to them, as is typically the case with sources of type I noise storm emission.

3.1. Noise storm sources

We have identified the brightest regions on the 169 MHz maps with faint noise storm continua, both because of their characteristics which are similar to those of the well studied brighter noise storms and because we observed type I bursts at the same location. Typical examples are the sources *A* and *B* in Figure 2, which are displaced by about 5 arc min relative to active regions. Their size is about 4 arc min by 6 arc min, which is slightly larger than the clean beam (1.5 by 4.2 arc min). The intensity of region *A* decreases from July 28 to August 1, from 1.55×10^6 K to the background level. Region *B* has a brightness temperature of about 10^6 K, except for August 1 when its temperature was 1.2×10^6 K; moreover between July 30 and 31 the region showed a small displacement toward the east. Since the noise storm continua are statistically brighter at the center of the disk than near the limb (Elgaroy, 1977), the intensity variations of the sources *A* and *B* must be real and not due to a center-to-limb effect. The presence of different components associated with the same active region, the systematic displacement with respect to the sunspots and the changes in intensity and location are classic characteristics of the much brighter noise storm centers (Le Squeren, 1963). Note that faint noise storm emission has also been observed by Sheridan (1970) and discussed by Riddle (1970).

Type I bursts above faint continua are not very frequent (a few dozen or less during six hours of observations). Using the high-time resolution (25 images s^{-1}) one-dimensional E–W and N–S data from the Nançay radioheliograph we measured the positions of type I bursts which we identified on the basis of their time profiles. On July 28 regions *A* and *B* produced several bursts, while on July 29 and 30 the only bursts detected by the radioheliograph were located in region *B*. No bursts were detected on July 31, from either region, while several type I bursts were observed from region *B* on August 1 and 2. Irregular bursting rate is a well known feature of bright noise storms. Moreover, since the location of sources *A* and *B* did not change significantly during the observing period (after taking into account the effects of rotation) we can conclude that their nature remains the same, even in the absence of detectable burst emission.

Other examples of noise storm sources can be found on the map of June 29, 1980 (Figure 3). A noise storm continuum (labeled *A'* on the map) is near the center of the disk and another one is near the west limb (*B'* in Figure 3). The latter showed important

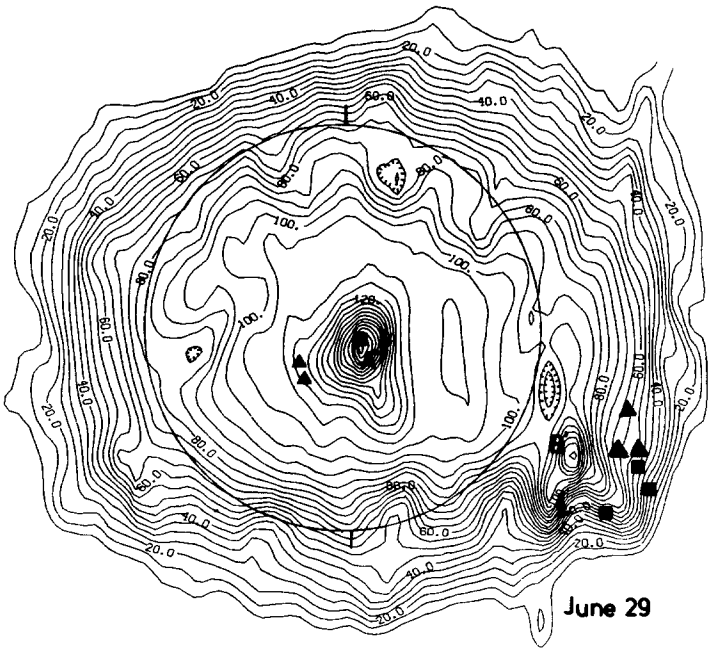

Fig. 3. Map of the Sun at 169 MHz on June 29, 1980, showing two sources of noise storm continua (A' and B'), the location of type I bursts (filled squares) and the locations of type III bursts (filled triangles). The part of the map west of the photospheric limb is partly distorted due to the variation of region B' during the observation.

intensity changes during the observations, consequently the western part of the map is distorted. The numerous type I bursts emitted by source A' between 09:03 UT and 09:50 UT were all at the same location (black square in Figure 3) while noise storm B' produced bursts around 10:50 UT which were located higher than the continuum source. The black triangles points show the positions of strong type III bursts observed around 10:40 UT near region B' (Raoult *et al.*, 1985) as well as the positions of faint type III bursts observed near region A′ around 14:35 UT.

The height of the sources above the photosphere, as well as their heliographic coordinates, can be computed from measurements of their position on consecutive days, assuming a rotation rate similar to that of photospheric features. Using the sunspot rotation rate and a least square fit we obtained values between 0.23 and 0.33 solar radii for the noise storms A, B, and A'; the accuracy of these values is about ± 0.1 solar radii. The average value is the same as the apparent height of source B' above the photospheric limb on June 29 (Figure 3).

As we discussed above, faint noise storm continua sometimes emit very few type I bursts and sometimes no bursts at all are detected during extended periods of time; therefore without high time resolution observations, the distinction between noise storms and other types of emission is difficult to make. Spectrographic as well as other full disk instruments are not sensitive enough to detect faint continua and weak isolated

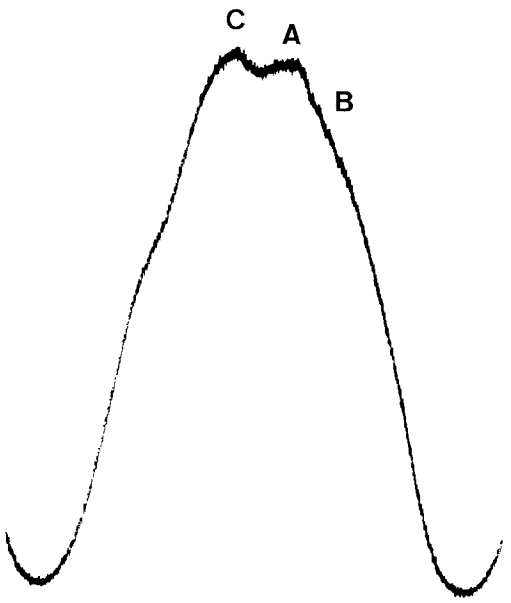

Fig. 4. One-dimensional east–west scan obtained on July 31, 1980 with the Nançay interferometer at 169 MHz. Labels *A*, *B*, and *C* show the location of the corresponding sources of the two-dimensional map of Figure 1.

type I bursts. Thus weak noise storms may have been included in previous studies of the slowly varying component. In Figure 4 we show the one-dimensional scan obtained with the Nançay east–west interferometer on July 31; this type of observations has been used by most authors for the study of the SVC at metric wavelengths until now. Labels *A*, *B*, and *C* how the projected position of the corresponding sources of Figure 2. It is clear that from interferometric observations alone it is impossible even to detect source *B*. It is also difficult to establish, on the basis of such observations, that *A* is a noise storm while *C* is not, although one might be able to identify faint noise storms if they show significant time variations during the observing period.

Consequently we suspect that studies of the SVC which have shown associations with spoted active regions may have been contaminated with faint noise storm continua of non-thermal origin. As in the case with the other noise storm emission, the faint continua are likely to be emitted in large scale corona arches with one leg anchored in active regions, as suggested by Lantos–Jarry (1970).

3.2. Emission features and the solar background

With the exception of regions *A* and *B* the localized emission sources in Figure 2 are not noise storm sources. Region *C* is the brightest of these sources; it is located far from active regions and no bursts were observed in that location during the period of our observations. As we mentioned above, such localized sources are not much brighter than the 'quiet Sun' background, their brightness temperature being between 5×10^4 and 2×10^5 K above the background. The average height of these sources, determined

from their rotation, is 0.23 solar radii; this value is slightly lower than that of noise storm sources, however the difference is within the error margin of the measurements.

For a more detailed study of these sources we show in Figure 5 the map of June 30, 1980. Noise storms A' and B' have been discussed in the previous section, while depressions will be discussed in the next section; the other emission sources are labeled with greek letters. The chromospheric features which are best associated with the 169 MHz sources are the neutral lines of the magnetic field as deduced, for example from Hα observations (McIntosh *et al.*, 1976; Space Environment Laboratory, 1980). On Figure 5, sources α, β, and γ are localized sources, while δ, ε, and ζ are rather part of the solar background emission; the overall shape of the latter appears to be associated with the neutral line topology. A further comparison of the sources with the strength of the photospheric magnetic field showed that the sources occur preferentially above neutral lines surrounded by medium, rather than low intensity field. No emission at 169 MHz is detected above regions with high magnetic field strength which correspond to active regions.

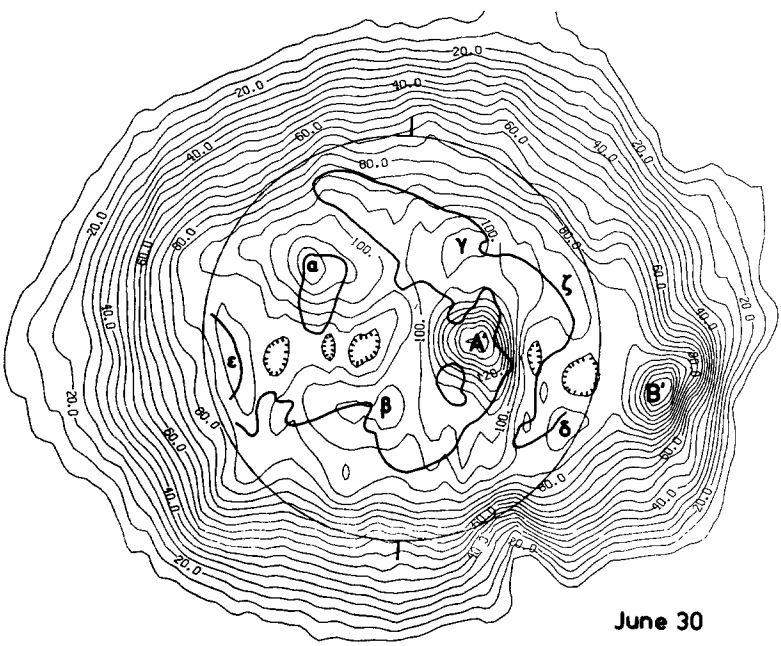

Fig. 5. Solar map on June 30, 1980 on which we have drawn the neutral lines of the photospheric magnetic field. The depressions near the equator correspond to regions *a* and *b* of Figure 7.

The picture that emerges from the associations of low intensity metric sources with neutral lines is compatible with the enhanced emission originating in coronal arch systems with higher temperature and/or emission measure than their surroundings, as observed in soft X-rays during the Skylab mission. However, this association needs to be further confirmed with a larger set of observational data; the main problem arises

from the fact that neutral lines cross practically the entire disk, consequently the identification of a source with a particular neutral line should be done with extreme care.

As we mentioned in Section 3 we have not detected any emission associated with large quiescent filaments. As for the association of localized metric emission with coronal streamers, we cannot make a detailed study because we do not have K-coronameter data. A comparison of polar plots of brightness temperature at a height of 0.15 solar radii with Sacramento peak observations of the green line (*Solar Geophysical Data*, 1980) is shown in Figure 6. The 169 MHz and the green line plots have roughly the same form, however there are differences in the small scale structure. Since the two emissions are affected in a different way by the electron temperature and density of the corona and, moreover the metric data may be affected by refraction we do not expect a one-to-one correspondence of the features. On the other hand, the metric maps do not show clear evidence of individual streamers at the limb, except perhaps for the structure at the east limb near the equator on July 30–August 1 (Figure 2). We should note, however, that due to instrumental limitations, our maps may not be very accurate at large distances from the photospheric limb (cf. Section 2).

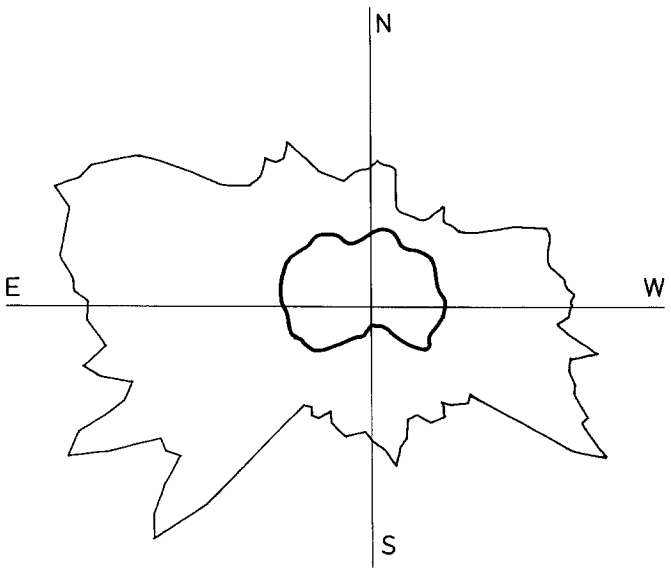

Fig. 6. Polar plots on August 2, 1980 of the brightness temperature at 169 MHz (heavy line) and of the intensity of the green line (Sacramento Peak Observatory) both at a height of 0.15 $R_{\odot}$ above the photospheric limb.

3.3. Coronal holes

According to the compilation of brightness temperature measurements by Lantos (1980), loop regions show a wide variation between 7×10^5 and 1.2×10^6 K. Consequently, depressions seen on the disk (e.g. Figure 2) are not necessarily coronal holes;

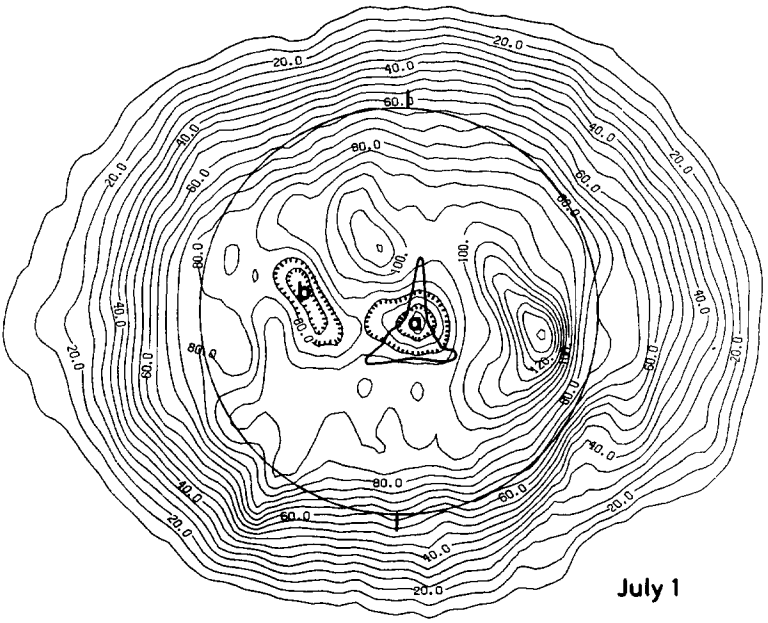

Fig. 7. Map of the Sun on July 1, 1980. The heavy line shows the boundary of a coronal hole on the basis of observations in the He I line at 10830 Å (Kitt Peak Observatory).

they might as well be loop regions with low electron temperature and/or low emission measure. On the other hand, since coronal holes were coherently observed to have a brightness temperature of $(6.4 \pm 0.8) \times 10^5$ K around 169 MHz, their identification on the maps can be partly based on the depth of the depression. The map of July 1, 1980 (Figure 7) shows a very deep depression at the center of the disk (labelled *a* in Figure 7), with a minimum brightness temperature of 6.8×10^5 K. Kitt-Peak observations at the He I line at 10830 Å (courtesy of J. Harvey) show evidence of a coronal hole at the same location. The boundary of the hole is drawn on Figure 7 as a heavy line; in comparing the shape of the region at 169 MHz and in He I one should take into account the considerably lower resolution of the metric map. The other depression (labeled *b* in Figure 7) which is observed to the east of depression *a* has a minimum brightness temperature of 7.2×10^5 K; it is located above a quiet region but has no specific counterpart in He I. This may also be a coronal hole. In any case we should note that there is not always a one-to-one association of He I emission features with X-ray coronal holes (Kahler *et al.*, 1983). Region *b* is visible in the June 29 map (Figure 3) near the east photospheric limb; both sources are seen on the map of June 30 (Figure 5) as well as on the maps of July 2 (Figure 8) and July 3. On the basis of their rotation and assuming a rigid rotation rate of 13.23 degrees per day (Howard, 1978) we computed an apparent height of 0.03 solar radii for depression *a* and 0.1 solar radii for *b*; although the concept of height is not well defined for holes and moreover the accuracy of these estimates is not better than 0.1 $R_\odot$, there is clear evidence that the radiation from these regions originates lower in the corona than that from emission sources.

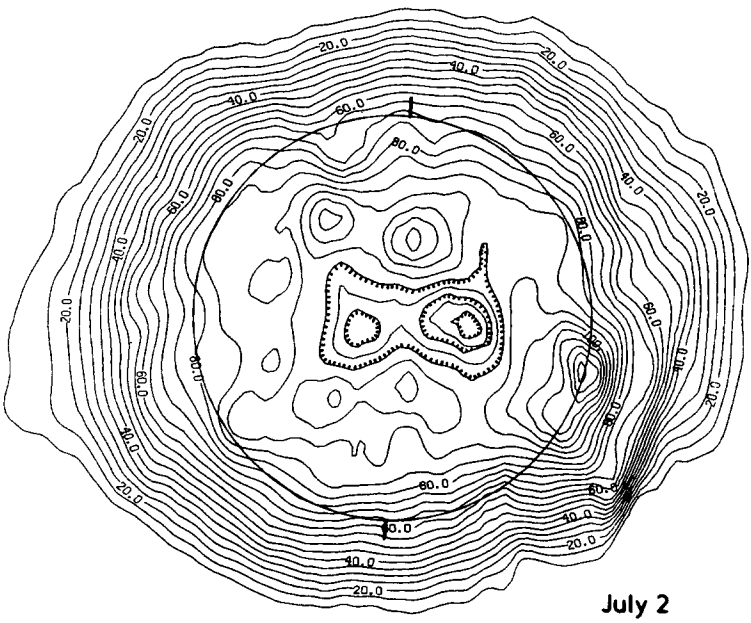

Fig. 8. Map of the Sun on July 2, 1980. The depressions near the center of the disk correspond to regions *a* and *b* of Figure 7.

Depressions are also observed far from the equator, such as the regions *D* and *E* in Figure 2. The northern depression appears on July 30, and is visible until the end of the observing period on August 5, while the southern depression is detectable from July 28 to 31. Both rotate with the Sun although their rotation is not quite regular, which could be due to the presence of emitting material in front of the holes. According to the He I data there is an intrusion of the south pole coronal hole up to a latitude of $-38°$ near the region where we observe depression *D*; this is not the case, however, with the north polar hole which extends down to a latitude of about $75°$ and shows no intrusion that might be associated with our depression *E*. The radio observations are quite sensitive to variations of emission measure and electron temperature, consequently the metric maps are in principle more suitable for the detection of coronal holes. The problem of confusion with low brightness arch regions is mainly due to the lower resolution of the radio data.

4. Summary and Conclusions

The use of the Nançay radioheliograph as a synthesis instrument has provided a new source of data for the study of solar features that are stable over an interval of about 6 hr at 169 MHz. Although the present study is based on a limited set of data we find strong evidence that some localized emission regions located near but not directly above active regions are actually sources of noise storm continua, while others appear to be

associated with regions of moderate magnetic field intensity along neutral lines and apparently correspond to coronal arch systems. The distinction between these two types of sources is difficult in the absence of high time resolution positional data which can provide information about the location of associated bursts. It is therefore possible that noise storm continua may have been included in past studies of the slowly varying component. Thus, the purely morphological definition of the SVC as the emission from sources rotating with the Sun may have to be reexamined, because such sources may either be part of quiet Sun emission (arches) or of burst emission (noise storms). It is clear that further observations are necessary in order to establish the properties of these two types of sources and interpret the origin of the emission.

Apart from the possible association with neutral lines, our observations do not show any obvious relationship of metric emission sources with optical features. In particular, during our period, we find no evidence of sources associated with large quiescent filaments.

Coronal holes are visible as deep depressions on our maps, both near the equator and around the poles. Shallower depressions may be quiet regions with lower than average electron temperature and/or emission measure. Again further analysis of more observations as well as simultaneous observations in other wavelengths is necessary for a better understanding of the coronal holes.

Finally the identification of streamers at the limb is not easy without *K*-coronameter data. Our observations show a rough agreement with coronal green line observations, but there are considerable differences in the details. Coronal streamers and their association with disk features can be studied better with the use of synoptic maps, which require considerably longer periods of continuous observations than the ones we studied here.

Acknowledgements

The authors wish to thank R. Stewart and J. Harvey for providing Culgoora maps and He I 10850 Å observations, respectively. One of the authors (C.E.A.) is grateful to the Radioheliograph Group of Meudon Observatory for their invitation, their warm hospitality, and their collaboration. This research is supported in part by the National Science Foundations of Greece, by the Paris-Meudon Observatory and the Centre National de la Recherche Scientifique.

References

Alissandrakis, C. E.: 1983, Internal Report, Meudon Observatory.
Axisa, F., Avignon, Y., Martres, M. J., Pick, M., and Simon, P.: 1971, *Solar Phys.* **19**, 110.
Chiuderi-Drago, F., Avignon, Y., and Thomas, R. J.: 1977, *Solar Phys.* **51**, 143.
Dulk, G. A. and Sheridan, K. V.: 1974, *Solar Phys.* **36**, 191.
Elgaroy, E. O.: 1977, *Solar Noise Storms*, Pergamon Press.
Formalont, E. B. and Wright, C. H.: 1974, in G. L. Verschmur and K. I. Kellerman (eds.), *Galactic and Extra-Galactic Radio Astronomy*, Springer-Verlag, Berlin.

Högbom, J. A.: 1974, *Astron. Astrophys. Suppl.* **15**, 417.
Howard, R.: 1978, *Rev. Geophys. Space Phys.* **16**, 721.
Kahler, S. W., Davis, J. M., and Harvey, J. W.: 1983, *Solar Phys.* **87**, 47.
Kundu, M. R.: 1965, *Solar Radioastronomy*, Interscience Publishers.
Kundu, M. R. and Alissandrakis, C. E.: 1975, *Nature* **257**, 465.
Kundu, M. R., Alissandrakis, C. E., Bregman, J. D., and Hin, A. C.: 1977, *Astrophys. J.* **213**, 278.
Lantos, P.: 1980, in M. R. Kundu and T. Gergely (eds.), 'Radio Physics of the Sun', *IAU Symp.* **86**.
Lantos, P. and Avignon, Y.: 1975, *Astron. Astrophys.* **41**, 137.
Lantos-Jarry, M. F.: 1970, *Solar Phys.* **15**, 40.
Leblanc, Y.: 1970, *Astron. Astrophys.* **4**, 315.
Le Squeren, A. M.: 1963, *Ann. Astrophys.* **26**, 97.
McIntosh, P. S., Krieger, A. S., Nolte, J. T., and Vaiana, G.: 1976, *Solar Phys.* **49**, 57.
Moutot, M. and Boischot, A.: 1961, *Ann. Astrophys.* **24**, 171.
Radioheliograph Group: 1977, *Solar Phys.* **55**, 251.
Radioheliograph Group: 1983, *Solar Phys.* **88**, 383.
Raoult, A., Pick, M., Dennis, B. R., and Kane, S.: 1985, submitted to *Astrophys. J.*
Riddle, A. C.: 1970, *Proc. ASA* **1**, 375.
Sheridan, K. V.: 1970, *Proc. ASA* **1**, 304.
Space Environment Laboratory, Boulder: 1980, private communication.
Trottet, G. and Lantos, P.: 1978, *Astron. Astrophys.* **70**, 245.